8-2-2010

In vivo analysis of CCM3, a gene involved in cerebral cavernous malformation development

Aimee Two

In vivo analysis of *CCM3*, a gene involved in cerebral cavernous malformation development

A Thesis Submitted to the
Yale University School of Medicine
in Partial Fulfillment of the Requirements for the
Degree of Doctor of Medicine

by

Aimee Two
2010

IN VIVO ANALYSIS OF *CCM3*, A GENE INVOLVED IN CEREBRAL CAVERNOUS MALFORMATION DEVELOPMENT.

Aimee Two, Angeliki Louvi, and Murat Gunel. Department of Neurosurgery, Yale University, School of Medicine, New Haven, CT.

Cerebral cavernous malformations (CCMs), one of the most common vascular malformations of the central nervous system (CNS), occur due to both sporadic and familial mutations in any of the three *CCM* genes: *CCM1*, or *KRIT1*; *CCM2*, or *malcavernin*; and *CCM3*, the *Programmed Cell Death 10* gene. As the most recently discovered of these genes, *CCM3* remains poorly understood. In vitro analysis has suggested a role for it in apoptosis, but in vivo studies of this gene are limited and thus are the goal of the current work. Using conditional knockout mice in which *Ccm3* has been inactivated in neural cells, experimental animals were created that develop lesions resembling human CCMs. In situ hybridization and immunohistochemistry were used to compare staining patterns of glial fibrillary acidic protein (GFAP) and vimentin, both expressed in astrocytes, with vimentin being expressed specifically in activated astrocytes, as well as connexin43, a gap junction protein that links astrocytic foot processes along the blood brain barrier (BBB), and aquaporin 4, a water channel expressed exclusively in astrocytes, between control and experimental brains. Results showed an increase in GFAP and vimentin expression in experimental brains, suggesting increased glial activation, but a decrease in that of connexin43 and aquaporin 4, suggesting an abnormality of these astrocytes. Given that CCMs represent endothelial

cell and not astrocyte pathology, these results suggest that lesion formation may be related to disrupted communication within the neurovascular unit.

ACKNOWLEDGEMENTS

First I would like to thank my mentors, Drs. Murat Gunel and Angeliki Louvi, for their guidance during my research year. I can't imagine the year being as productive or educational without their encouragement and expertise.

I would also like to thank my parents for their unconditional support throughout my education. Thank you for your encouragement, for teaching me to always strive to reach my goals, and for always believing in me.

Finally, thank you to Yale University School of Medicine for funding my research. My year in the lab would not have been possible without the support of the Yale One Year Medical Student Fellowship.

TABLE OF CONTENTS

INTRODUCTION

Cerebral cavernous malformations (CCMs), or cavernomas, are low-flow vascular lesions most commonly found in the central nervous system (CNS). They consist of a compact mass of abnormally dilated vascular channels lacking intervening neural parenchyma. The vascular channels comprising these lesions resemble capillaries in that they consist of a single endothelial layer and lack structural elements such as elastin and smooth muscle normally found in the walls of other vessels. Unlike capillaries, however, these vessels are "leaky," allowing for frequent microhemorrhages that permit blood to escape into the surrounding brain tissue [1]. In addition to hemorrhaging, these lesions can thrombose, which also causes lesion expansion, and, if significant, can compress nearby brain structures. When grossly examined, malformations are raspberry-like in appearance and range in diameter from one millimeter to several centimeters. In addition to the CNS, these lesions can occasionally be seen in most other organ systems of the body, including the skin and eye.

Before the advent of MRI, CCMs were thought to be rare lesions. Radiographic techniques at that time failed to properly diagnose these malformations, and thus CCMs were only detected after surgical resection or during autopsies. The first study to suggest

a higher than expected prevalence of CCMs was an autopsy-based report published in 1989 suggesting a prevalence of 0.4% [2]. This finding was confirmed soon after by MRI-based studies that suggested the prevalence of CCMs to range from 0.4 to 0.9% [3, 4]. Given these statistics, CCMs are now recognized as a relatively common vascular malformation afflicting one in approximately 200 individuals and comprising 8-15% of vascular malformations of the CNS [5, 6].

One of the main reasons the recognition of CCMs as a common vascular lesion required autopsy- and MRI-based studies is because of the disease's clinical presentation. Only 20-30% of patients with CCMs experience lesion-related symptoms during their lifetime, and thus most never present to healthcare providers [3]. Those that do present for medical attention usually do so during their 3rd to 5th decade of life after experiencing such symptoms as headaches, seizures, and focal neurologic deficits [3]. Life-threatening intracerebral hemorrhages can also occur, but are extremely rare, occurring in 0.25% to 6% of patients [7-9].

The onset of symptoms in patients with CCMs is always related to some change in the lesion itself. Given the leakiness of the vascular channels comprising these lesions, microhemorrhages are common, and thus blood frequently extravasates from these lesions into the surrounding neural parenchyma, where it is metabolized over a period of days to weeks [10]. Blood break-down products accumulate in the surrounding brain tissue during this time and can serve as a focus for seizure activity. Aside from these

long-term consequences, microhemorrhages are often clinically silent. Their high frequency helps explains why seizures are the most common presenting symptom for CCMs [11, 12].

The remainder of symptoms associated with cavernomas is attributable to lesion expansion. Lesion expansion can occur through one of two means: gross hemorrhage or lesion thrombosis [10]. With a gross hemorrhage, a significant amount of blood escapes from the lesion at a rate that cannot be accommodated by the closed intracranial space. Similarly, when a thrombus forms within a lesion, the lesion becomes congested with blood and swells. If the intracranial space cannot accommodate the swelling, symptoms ensue due to the resulting mass effect. Additionally, the increased pressure seen upstream of a clot in a cavernoma can cause rupture of the lesion and thus gross hemorrhage [13]. Since cavernomas generally represent a low-pressure, low-flow state, though, large bleeds are relatively uncommon. Although the annual rate of clinically significant hemorrhages can vary greatly among patients, it is generally thought to range from 2 to 5% [14].

Another common presentation of CCMs is through incidental detection on imaging studies performed for unrelated reasons. As previously discussed, the increasing use of MRI has allowed for detection of lesions that otherwise would have remained undiagnosed [3, 4]. Despite advances in CCM detection, however, treatment options for these potentially devastating lesions unfortunately remain limited. Complete surgical

resection is the only true cure for CCMs, but this option is not available to all patients. Older patients or those with significant co-morbidities may not be appropriate candidates for undergoing the often extensive procedure of CCM removal. In such cases, the risks of surgery outweigh its potential benefits, and thus an alternative treatment must be sought. Similarly, the location and surgical accessibility of a lesion also must be considered when planning treatment. CCMs in or near eloquent brain structures or in regions that cannot easily be reached surgically may not be amenable to resection. Finally, patients with the familial form of the disease may have upwards of hundreds of lesions, and thus surgery on all of them would be impossible.

For patients in whom surgery is not an option, alternative management strategies are limited. Medical management can be used for seizure control, but aside from alleviating this symptom, pharmacologic agents have no role in the treatment of cavernomas. Even when anti-epileptic drugs are used, though, seizures are not always relieved. Since the seizure focus in patients with CCMs is usually hemosiderin that has accumulated in the brain tissue surrounding lesions after repeated microhemorrhages, anti-epileptic drugs fail to eliminate the source of seizures in these patients. These medications therefore merely increase the seizure threshold of the local tissue, which can be completely curative for some patients, but leaves others still to experience symptoms, at times even despite the use of multiple agents. For these patients with refractory seizures causing significant impairment in a patient's life, surgery would again be the recommended treatment option.

For patients not receiving either surgical or medical management, expectant management is the preferred option for managing CCMs. This strategy is preferred for patients with lesions that are not surgically accessible, as well as for asymptomatic patients in whom the benefits of surgery may not outweigh the risks. Under this management plan, patients are followed with serial MRIs every year or two, and new scans compared to older ones for any evidence of lesion enlargement or hemorrhage. If the scan shows no new changes to the lesion, the patient can continue to be followed expectantly. If changes are present, though, intervention may be necessary, which then leaves patients with surgery as their only option.

Although radiosurgery has also been suggested as a treatment option for CCMs, most of the available literature on this topic fails to show a clear benefit of this procedure. While some studies report decreased hemorrhage rates following radiosurgery [15, 16], others, including some of these same studies, show an increased complication rate following this treatment, including permanent neurological deficits [17-19]. Patients in one study also had to undergo surgical resection of their lesions after radiosurgery due to its inability to completely thrombose the cavernoma [18]. This finding prompted histological studies of lesions resected from patients who had previously undergone radiosurgical treatment of their cavernomas. The specimens in these studies were not occluded, suggesting that radiosurgery fails to adequately treat these lesions [20]. For these reasons, the use of radiosurgery as a treatment for CCMs remains a topic of much controversy.

As the only truly curative option for CCM management, surgery is therefore the preferred treatment option for these lesions. Such an intervention is not without risks, though, and these can range from permanent focal neurologic deficits to death. Given the limited treatment options for CCMs as well as the potential risks of such an operation, it is clear why better treatment options for cavernomas must be sought. In order to accomplish this goal, though, further understanding of the disease, including its underlying molecular mechanisms, is necessary.

As a genetic condition, the heritable nature of cavernomas has been recognized since the disease's original description, and this feature has played a large role in allowing for significant advances in elucidating the underlying molecular pathophysiology of these lesions [21]. Although sporadic mutations contribute to the majority of the disease's prevalence, 10-50% of cavernomas are inherited [22, 23]. Familial CCMs are inherited in an autosomal dominant fashion with a high degree of penetrance, making it a relatively common genetic disorder in afflicted families. Through genetic linkage analyses using afflicted families, three loci were discovered to play a role in the development of these lesions [24-28]. Subsequent positional cloning experiments identified the three genes that lie within those loci as *CCM1*, *CCM2*, and *CCM3*. Together mutations in these three genes are thought to account for 96% of familial cavernomas [29].

CCM1, or Krev1 interaction trapped protein-1 (*KRIT1*), lies on chromosome 7q21 and contains 16 exons that encode the 736 amino acid protein KRIT1. Over 80 different

mutations in this gene have been found that lead to clinically evident CCMs, including one that is responsible for over 90% of familial cases in Hispanic-American patients. Almost all of these mutations are nonsense mutations in which a premature stop codon or a frameshift mutation results in premature termination of translation [30-35], providing evidence that disease is caused by a loss-of-function mutation and suggesting a two-hit mechanism of disease development [36]. The first "hit" in this case would be an inherited germ line mutation, and the second "hit" acquired in affected cells.

As the first of the CCM genes to be identified, CCM1's function has been studied in great detail. Its resulting protein, KRIT1, has been found to have several domains implicated in protein-protein interactions, including one, a FERM domain, that is typically critical for binding to the cell membrane [37]. It also contains a series of ankyrin repeats, whose interactions remain unknown, as well as 3 NPXY domains through which it is thought to associate with Integrin Cytoplasmic domain-Associated Protein-1α (ICAP-1α) [38, 39] and CCM2 [40]. ICAP1α is known to bind to β1 integrin [41, 42], and integrins, specifically β1 integrin, are important proteins that regulate endothelial cell adhesion and migration throughout angiogenesis [43, 44]. These findings therefore suggest a role for CCM1 in vascular development, a result that is confirmed by in vivo analysis.

Interactions between CCM1 and CCM2 have also been studied extensively. Results have shown that these two molecules bind not only to each other, but also to CCM3 [45, 46]. Although the exact role of this complex is not known, CCM2 appears to play a

scaffolding role [47], potentially being recruited to cell-cell junctions through its interactions with CCM1.

KRIT1 is expressed in many human tissues, but most relevant to CCM pathology is its presence in neurons, astrocytes, and the endothelium of arteries and capillaries [48]. Consistent with this localization, in vivo studies suggest that CCM1 plays an essential role in vascular development. *Ccm1* knock-out mice are embryonically lethal due to vascular defects incompatible with life. Post-mortem analysis of these embryos demonstrates an enlarged caudal dorsal aorta, dilated brain precursor vessels, and variable obstruction of branchial arch arteries and the proximal dorsal aorta [49]. In contrast, $Ccm1^{+/-}$ animals survive embryogenesis and are phenotypically normal. Crossing them with $p53^{-/-}$ mutants, however, results in development of vascular lesions resembling cavernomas in about 55% of $Ccm1^{+/-}$ $p53^{-/-}$ animals [50]. Although the mechanism underlying the enhanced phenotype in the absence of p53 is not known, it is speculated to be due to increased rate of somatic mutations leading to more second hits and thereby resulting in the formation of CCM lesions in the compound animals. Nonetheless, these findings once again implicate CCM1 in the development of these vascular lesions.

The *CCM2* gene is *MGC4607*, or *malcavernin*. *MGC4607* is a ten exon gene located on chromosome 7p13 and encoding the CCM2 protein. Almost all CCM2 mutations in affected patients are nonsense mutations, resulting from premature stop codons or frameshift mutations that imply loss-of-function of CCM2 as the cause of the resulting

pathophysiology. The expression pattern of CCM2 is similar to that of CCM1, localizing to neurons, astrocytes and the arterial endothelium. Although its function is not completely known, CCM2 has significant homology to OSM, a protein in rodents that is responsible for osmo- and mechano-sensing of the extracellular matrix. In humans, CCM2 plays a role as a scaffolding protein, using p38 signaling to convey information about environmental stress [47]. In addition, in vivo studies predict that CCM2 has a major angiogenic role since *Ccm2* knock-out mice, like the *Ccm1* mutants, die during embryogenesis due to gross vascular defects [49, 51].

Most recently, *PDCD10*, or *Programmed Cell Death 10* was identified as being the causative gene in CCM3 families. This seven exon gene is located on 3q26 and encodes a 212 amino acid protein. Interestingly, CCM3 also shares the expression pattern of CCM1 and CCM2, being present in the arterial portion of the endothelium as well as neurons and astrocytes [52]. In vitro studies of CCM3 suggest that it is both necessary and sufficient to induce apoptosis [53]. However, being the most recently identified, the least is known about this gene.

Gaining further insight to the *CCM3* gene is critical for better understanding the pathophysiology underlying this disease. Although the gene's in vitro role in apoptosis has been clearly defined, its in vivo function remains to be elucidated. Like *Ccm1* and *Ccm2* knock-out animals, *Ccm3* complete knock-outs are embryonical lethal due to vascular defects (Y. He, H. Zhang, L. Yu, M. Günel and W. Min: PDCD10/CCM3 is

critical for vascular development by regulating VEGFR2-MEKK3-MAPK signaling, *submitted*). Therefore, to further understand this gene's role in vivo, cell-specific conditional *Ccm3* knock-out mice were generated in which*Ccm3* was selectively inactivated in specific cells of a particular lineage using different promoters to drive Cre recombinase. Given that CCMs are vascular lesions, the first such conditional knock-outs targeted the vascular system using Tie-2, a promoter specific to endothelial cells [54]. Animals with this mutation did not survive embryogenesis, though, as they died between embryonic days 9 and 10 of gross vascular defects. The brain was the next organ system targeted since this is the location where lesions are most commonly seen, and two different promoters were used to selectively inactivate *Ccm3* in different neural cell lines. In one, glial fibrillary acidic protein (GFAP) was used to target radial glial cells, and in the other, Emx1 was used to target dorsal telencephalic progenitor cells. More specifically, GFAP is expressed in radial glial cells and their progeny, including neurons and astrocytes of both the cerebral and cerebellar cortices [55, 56], and Emx1 is expressed in telencephalic neuronal progenitors, including neurons of the neocortex and hippocampus as well as astrocytes and oligodendroglia [57]. Not only do animals in both of these experimental strains survived embryogenesis, but many, including most of the Emx1 animals, survived through the weaning process and into adulthood, allowing for characterization of these animals' brains at various stages of postnatal development.

STATEMENT OF PURPOSE AND HYPOTHESIS

The goal of this research is to examine the role of *CCM3* in brain development and in the pathophysiology of CCMs using an animal model in which *Ccm3* has been selectively inactivated in neural cells in the CNS of mice. These mutant brains will be examined for gross morphology, cytoarchitecture and expression of cellular markers, and these results compared to those of control brains.

Since the in vivo role of *CCM3* has yet to be determined, it is difficult to predict the ways in which mutant brains will differ from those of controls. *CCM3*'s role in vitro has been established as being both necessary and sufficient for induction of apoptosis, though, so one possibility is that it plays a similar role in vivo. Were such an occurrence to be true, it is hypothesized that mutant brains would be marked by increased cellularity of both neurons and astrocytes, the cell types in which *Ccm3* has been deleted. This change could potentially result in larger brains in experimental animals, as well as structural disorganization given that apoptosis plays a role in cortical organization during neurodevelopment. It is also possible that experimental animals will develop cavernoma-like lesions since *CCM3* mutations in humans cause CCMs, but the likelihood of this occurrence remains uncertain given that cavernomas are vascular lesions and that *Ccm3* is selectively inactivated in neural and not endothelial cells in this experimental model. If CCMs are seen in mutant brains, however, this finding would suggest a non-cell

autonomous role of CCM3 in neural cells that affects the neurovascular unit and the communication occurring between its components, affected neurons and the vasculature. Such an occurrence would also potentially implicate disrupted communication within this unit as being responsible for lesion formation.

METHODS

Animal Care

All animals used in this study have been previously described by other groups. *GFAP*-Cre (GFAP) and *Emx1*-IRES-Cre (Emx1) mice were obtained from Jackson Laboratories. *Ccm3*^{lox} mice were obtained from Dr. Wang Min, Department of Pathology, Yale School of Medicine (He et al., *submitted*). All mice were maintained in a mixed genetic background (C57BL6, 129, FVB). They were bred by one of the lab's principle investigators, who ensured that all breeding and maintenance occurred in compliance with National Institutes of Health guidelines. The Yale University Institutional Animal Care & Use Committee approved the animal protocols used.

Genotyping

Animals were genotyped within the first two weeks of postnatal development. This responsibility was shared amongst lab members, and as such was completed by students and research assistants in the lab, as well as by the principle investigator. The first step in this process was to extract DNA from the animal using a clipping from its tail. Tails were collected in 1.5-milliliter (mL) Eppendorf tubes. 100 microliters (µL) of 50mM NaOH was added to each Eppendorf tube, and tubes were then placed at 90 C. After 30 minutes, tubes were removed from the heat and immediately placed on ice. They were then centrifuged at 13.2 g for 30 seconds. 30 µL of 1M Tris buffer was then added to

each tube, and tubes vortexed briefly. The resulting DNA suspension was either used immediately or stored at 4 C until ready to be used for genotyping.

All genotyping protocols were completed using a set of DNA primers complementary to the genomic DNA sequences of interest, which for this study included Cre and Ccm3 lox. These sequences were then amplified using a polymerase chain reaction (PCR) protocol specific for each set of primers, and gel electrophoresis used for detection of PCR products. Animals containing both Cre and $Ccm3^{lox/lox}$ were considered experimental animals. All other animals were considered as controls, after initial analyses demonstrated that Cre^{+};$Ccm3^{lox/+}$ animals were indistinguishable from non-Cre controls.

Weights

Body weights were measured on a digital scale after anesthetizing animals but prior to intracardiac perfusion. Brain weights were also measured on a digit scale, but measurements were made after brains were dissected from the animal's skull and all membranes removed. Weighs were taken by various lab members, including the author of this manuscript.

Electron Microscopy

Electron microscopy was performed by one of the lab's principle investigators in order to analyze the ultrastructural characteristics of vascular lesions. Prior to doing so, animals

were deeply anesthetized using intracardiac injections of 2.5% glutaraldehyde and 2% paraformaldehyde in 0.1M sodium cacodylate buffer (pH 7.4). Brain tissue was then dissected, rinsed, and dehydrated in a series of ethanol dilutions (50-100%) before embedding in epoxy resin (Embed 812; Electron Microscopy Sciences). Tissue was then sectioned in the coronal plane at 60 nm on a Reichert ultramicrotome and collected on Formvar- and carbon-coated grids. The samples were stained with 2% uranyl acetate and lead citrate and examined on a Philips Tecnai 12 BioTWIN electron microscope (FEI Co.). Images were captured digitally using a CCD camera (Morada; Soft Imaging System, Muenster, Germany).

In Situ Hybridization

All in situ hybridization was done using riboprobes made by the author of this manuscript. The process for creating riboprobes, as well as the staining protocol used for the in situ studies, are described below.

Riboprobe creation

Gene Cloning: Primers for each gene of interest were created using the program Primer3 and then ordered from commercial sources. Using these primers and mouse cDNA, the gene of interest was amplified using a touchdown PCR protocol. The

resulting PCR products were run on an agarose gel to ensure products were of the expected nucleotide length based on the Primer3 results. Appropriately-sized PCR products were then transformed into competent E. coli cells, plated, and plates left to grow in an incubator overnight at 37 degrees. The next day, colonies were selected for insert amplification using M13 forward and reverse primers. Colonies with amplification products that matched our expected insert size were then grown overnight in liquid culture tubes containing 2 mL of Luria broth (LB) with ampicillin. The next morning, 1.5 mL from each of these cultures were transferred to an Eppendorf tube, and the remaining 0.5 mL was left at 4 C as a temporary stock solution. Each Eppendorf tube was then centrifuged at 8,000 g for 3 minutes. The supernatant was then carefully removed from each tube so as not to disturb the bacterial pellet. Next, the DNA from each pellet was purified using Quiaquik's Miniprep protocol (available online at http://www1.qiagen.com/literature/handbooks/literature.aspx?id=1000248). At the end of this protocol, the DNA was eluted from the Quiaquik column using 50 uL of Buffer EB, and the concentration of the resulting DNA measured using the program NanoDrop. Approximately 600 ng of plasmid DNA was then digested in a 10 mL EcoRI digestion assay using 0.5 uL EcoRI restriction enzyme and 1 uL of 10X EcoRI buffer. After a 1.5 hour incubation at 37 degrees, the assays were run on an agarose gel. DNA from each corresponding lane in the gel that contained DNA fragments of the expected size was then sent for sequencing at the W.M. Keck Facility in New Haven, CT. Once nucleotide sequences were returned from the Keck Facility, they were compared to the mouse genome using the National Center for Biotechnology Information's Basic Local

Alignment Search Tool. Sequences with greater than 95% homology to the gene of interest were considered to be cloned accurately.

Sequences of accurately cloned genes were entered into NEBcutter V2.0 (New England Biolabs, http://tools.neb.com/NEBcutter2/index.php) to determine which restriction enzymes would cut the DNA in the desired location in order to linearize it.

Riboprobe Template Creation: In order to create more DNA for the genes that were correctly cloned, new liquid cultures were grown from the temporary stock solution. The Quiaquik Miniprep protocol was once again used to purify DNA from these cultures. 20 ug of the resulting purified plasmid DNA was then linearized in a 100 uL digestion assay using the appropriate restriction enzyme per the results provided by NEBcutter V2.0. Resulting products were run on an agarose gel to ensure that linearization was complete. Extra proteins were then digested using proteinase K. A phenol/chloroform extraction was then used to extract the riboprobe template. The template was then precipitated with sodium acetate, washed with 70% ethanol (EtOH), and re-suspended in 20 uL DEPC-H_2O for a total concentration of 1 ug/uL.

Riboprobe finalization: A transcription reaction was then used to create the antisense riboprobe from the linearized template. After the reaction had run for 2 hours at 37 C, the probe was precipitated using 100 uL DEPC- H_2O, 10 uL of 4 M lithium chloride, and

300 uL 100% isopropanol. This reaction was incubated on ice for 15 minutes, and the supernatant decanted. The pellet was washed with 200 uL 70% EtOH, and centrifuged at 14,000 rpm at room temperature for 5 minutes. The supernatant was again decanted and the pellet allowed to dry at room temperature before being re-suspended in 100 uL DEPC- H_2O.

In order to prepare for *in situ* hybridization, 70 uL of the antisense riboprobe was added to an RNase-free mailer containing 14 ml of hybridization solution. The solution was then mixed well and stored at -20 C until ready for use.

Tissue Preparation

Animals were anesthetized using subcutaneous injections of ketamine (100 mg/kg) and xylazine (10 mg/kg). Once deeply anesthetized, animals were perfused with an intracardiac injection of 10 mL of normal saline, followed by 10 mL of 4% paraformaldehyde (PFA). The animal's brain was then dissected from the skull and post-fixed for a minimum of 36 hours in a solution of 30% sucrose / 4% PFA before sectioning in the coronal plane on a Leica sledge cryomicrotome at 36 µm (Leica Microsystems, Germany). Sections were then mounted on superfrost slides and left to dry overnight at room temperature.

Staining Protocol

The following staining protocol was used for all in situ hybridization experiments. It was completed by both the author of this manuscript as well as one of the lab's principle investigators.

Day One:

1. Place slides with mounted sections in RNase-free mailers. Fix tissue in 4% PFA for 15 minutes.
2. Wash slides in DEPC-PBS 3 times, 5 minutes each wash.
3. Incubate twice in detergent solution, 15 minutes each time for tissue from animals ages 1-20 days, 30 minutes each time for animals older than 20 days.
4. Wash slides in DEPC-PBS for 10 minutes.
5. Incubate in proteinase K solution (1ug/ml).
6. Fix in PFA for 15 minutes.
7. Wash slides in DEPC-PBS 3 times, 5 minutes each wash.
8. Place slides in mailer containing desired hybridization solution. Incubate at 70 C overnight.

Day Two:

1. Wash slides three times in Solution X at 70 C for 45 minutes each wash.
2. Wash slides 3 times in TBST for 15 minutes each time.
3. Block tissue for 1 hour in 10% lamb serum in TBST.
4. Incubate tissue in preabsorbed anti-dig antibody diluted to 1:5000 in 1% lamb serum in TBST for 2 hours.
5. Wash three times in TBST, 15 minutes each wash.
6. Incubate overnight in color solution (made by adding 35 uL NBT and 35 uL BCIP per 10 ml NTMT) in the dark, or until color has finished developing. Color development is complete when tissue sections are stained with only a minimal amount of background staining. Staining for corresponding control and experimental tissue should continue for equal amounts of time.

7. Once the color has finished developing, wash slides in TBST to remove background.
8. Dehydrate slides (see protocol below) before coverslipping in Aquamount and allowing to dry overnight.

Sections were analyzed using a Zeiss AxioImager (Zeiss, Oberkochen, Germany) fitted with an AxioCam MRc5 digital camera. Images were captured using AxioVision software (Zeiss) and assembled in Adobe Photoshop.

Immunohistochemistry

Immunohistochemistry was performed by both one of the lab's principle investigators as well as the author of this manuscript using 3,3'-diaminobenzidine (DAB) staining. The protocols for both tissue preparation and staining are provided below.

Tissue Preparation

Animals were anesthetized and perfused, and their brains dissected from the skull as described previously for in situ hybridization. Brains were then post-fixed for a minimum of 36 hours in a solution of 30% sucrose in PBS before sectioning in the coronal plane at 40 µm.

Staining Protocol

All steps were performed in scintillation vials on a rocker at room temperature unless otherwise noted.

1. Wash sections 5 times for 5 minutes each in PBS.
2. Apply 1% H_2O_2 for 10 minutes.
3. Wash sections extensively 4 times for 15 minutes each in PBS.
4. Apply blocking solution with Triton X-100 for 1 hour
5. Dilute antibody in blocking solution with Triton X-100. Keep sections in antibody for 2 nights at 4 C.
6. Wash sections 4 times for 10 minutes each in PBS.
7. Apply secondary antibody diluted 1:250 in blocking solution without Triton for 2 hours.
8. Wash sections 4 times for 10 minutes each.
9. Prepare ABC mixture (Vector Laboratories) 30 minutes before applying. Put on rocker for 10 minutes, then apply to sections for 2 hours at room temperature.
10. Wash sections extensively four times for 15 minutes each time
11. Apply 0.05% DAB, pH 7.4 for 20 minutes in the dark. Then add 4 uL NH4CL (solution: 10% in d H_2O), 1 uL glucose oxidase (solution: 8 mg/ml in d H_2O), 10 uL Nickel-ammonium sulfate (solution: 1% in d H_2O) and 20 uL 10% glucose. Allow solution to develop in darkness, checking level of staining every 5 minutes until signal is fully developed.
12. Wash sections quickly in PBS, then again for 15 minutes, still in darkness.
13. Mount sections on slides and allow to dry overnight.
14. Dehydrate slides and coverslip using Aquamount.

Sections were then analyzed, and images captured as described above for in situ hybridization.

Slide dehydration

Prior to coverslipping with Aquamount, all slides were dehydrated by passing through the following sequence of solutions for 1 minute each:

1. Double distilled H_2O (ddH_2O)
2. 70% EtOH
3. 80% EtOH
4. 90% EtOH
5. 95% EtOH
6. 100% EtOH
7. 100% EtOH
8. Histoclear
9. Histoclear

Cresyl Violet Staining

Slides with dried sections were placed in a mailer containing 4% PFA for 15 minutes. Next, slides were rinsed with PBS twice, for 5 minutes each time. Slides were then transferred to a slide holder and passed through each of the following solutions for one minute sequentially: ddH_2O, 70% EtOH, 80% EtOH, 90% EtOH, 95% EtOH, 100% EtOH, 100% EtOH, and xylenes. The slides were then left in a second xylene solution for 30 minutes. After this step, they were transferred back to the first xylene solution, followed by 100% EtOH, another 100% EtOH solution, 95% EtOH, 90% EtOh, 80% EtOH, 70% EtOH, and ddH_2O for one minute each. The slides were then transferred to the staining solution at 42 C for 5 minutes, followed by a 5-minute wash in ddH_2O to remove excess staining solution. 3 drops of acetic acid were then added to 70% EtOH, and the slides were transferred to this solution until good contrast was seen between axon

tracts and cell bodies (about 5-10 minutes). Slides were then dehydrated using the Slide Dehydration protocol above before coverslipping with Eukitt.

RESULTS

Postnatal development

GFAP-Cre;Ccm3$^{lox/lox}$ animals

These animals complete embryogenesis and are born in expected Mendelian ratios. The majority of animals fail to thrive following the weaning process, however, and approximately 80% die before their fourth postnatal week of life ($n > 100$). These animals developed an unsteady gait and frequently adopted a circling behavior suggestive of vestibular abnormalities. Experimental animals are noticed to be smaller than their control littermates starting around the first week of postnatal life. By week three they are noted to have a body weight that was less than 50% of that of controls. Their brains, however, are larger than those of controls. This difference in brain weights is first seen starting around the second week of postnatal life, when the average brain weight of control animals is 0.55 g, and that of experimental animals is 0.48 g. These differences in both brain and body sizes between control and experimental animals persist throughout development and into adulthood, where the differences are significant ($p<0.01$ for brain weights of adult control versus experimental animals, as well as for body weights of adult control versus experimental animals) using a Student's t-test (Figure 1, Tables 1 and 2).

When sliced coronally, the cortex of experimental brains also appeared to be much thicker than those of control animals.

Emx1-Cre;Ccm3$^{lox/lox}$ animals

As with *GFAP-Cre;Ccm3*$^{lox/lox}$ animals, these animals survive embryogenesis and are born in expected Mendelian ratios. Unlike the *GFAP-Cre;Ccm3*$^{lox/lox}$ animals, though, these animals all survive the weaning process. Neither gait instability nor circling behaviors are noted, likely accounted for by the sparing of cerebellar cells in this experimental model. Although these animals are also noted to have decreased body weights and increased brain sizes when compared to control animals across development, these findings were not recorded and will not be presented in this work. Also like *GFAP-Cre;Ccm3*$^{lox/lox}$ animals, coronal sections through brains of *Emx1-Cre;Ccm3*$^{lox/lox}$ animals demonstrated a thickened cortex when compared to those of controls.

Lesion Detection

Blood-filled vascular lesions resembling human cavernomas were noted in animals of both strains upon postmortem brain analyses (Figure 2). Although most animals with lesions had just one lesion, animals were rarely seen that had two, and one animals with

even three, lesions. Among the GFAP-Cre conditional animals, lesions were observed in 67% (20/30) of animals that were studied. The earliest lesions to be detected were seen during postnatal week three, and all six animals with early lesions seen between three and eight weeks of age also had significant hydrocephalus. Eight Emx1 animals were also analyzed for CCMs, with the youngest of these animals being nine months of age and the oldest being 16 months. Lesions were seen in over 80% of these animals. All lesions detected were in brain structures expressing either the GFAP or Emx1 promoter, and therefore in regions subject to CCM deletion. For GFAP animals, these regions included the cerebral cortex, olfactory bulb, midbrain, pons, medulla and cerebellum. Affected areas in Emx1 animals included the cerebral cortex and olfactory bulb.

Lesion Analysis

Lesions were examined using antibody staining as well as electron microscopy to determine their composition and to compare it to that of human cavernomas. An antibody directed towards PECAM, a marker of endothelial cells, was applied to brain sections containing lesions. After staining, resulting lesions appeared to consist of multiple dilated channels outlined by a single layer of stained cells, suggesting a single endothelial cell layer comprising the sinusoids of lesions (Figure 3A). In situ hybridization for Igf2, a marker of mesenchymal cells, was also done on cavernoma-containing brain sections. Sections failed to demonstrate staining in the region of the lesion, but did show staining around the lesions, as well as throughout the remainder of

brain sections, suggesting the CCMs to be devoid of intervening parenchyma (Figure 3B).

Next, electron microscopy was used to determine ultrastructural characteristics of the lesions. This technique again identified a single layer of endothelial cells forming the vascular channels that comprise lesions. These cells are surrounded by a generally intact but irregular basement membrane, with collagen supporting the other side of this membrane. Tight junctions are seen separating endothelial cells. Erythrocytes and platelets are seen within the lumens of lesions, and erythrocytes are additionally seen abluminally (Figure 4).

Cytoarchitecture

Nissl staining was used to evaluate the cytoarchitecture of animals' brains. This protocol stains rough endoplasmic reticulum, allowing for detection of cell bodies. Two main differences were seen when comparing the Nissl staining results of control and experimental animal brains. The first of these differences was noticed in the cerebral cortex. Unlike control animals, which have clearly defined cortical layers, the cerebral cortex of experimental animals was disorganized and lacking structure. No discrete cortical layers could be distinguished.

The other main difference between the brains of these two groups of animals was seen in the hippocampal formation. While this structure in control animals consisted of a discrete line of tightly packed cells, in experimental animals this strict organization was lacking. Cells in the hippocampal formation of experimental animals were loosely arranged, giving this structure an appearance as if was blurred since it lacked the sharp discrete contours seen in controls. This observation held true for both GFAP and Emx1 strains of experimental animals (Figures 5 and 6).

Finally, an observation made only in brains of the GFAP animals was the disorganization of the cerebellum. Compared to the cerebellum of control animals, that of GFAP animals lacked a tight cellular alignment and clear definition along the folia of the cerebellum (Figure 7). This difference is not seen in the cerebellum of Emx1 mutant animals because this brain region is not targeted by the Emx1 promoter.

GFAP/vimentin Staining

Both GFAP and vimentin stain intermediate filaments in astrocytes, with GFAP being expressed generally in astrocytes and vimentin being expressed in a cytoskeletal element seen only in activated (reactive) astrocytes. Staining for both of these markers using in

situ hybridization was used to compare the presence of astrocytes in adult control animal brains to that of adult experimental animal brains. GFAP staining in control animals was darkest in structures containing mostly white matter, and otherwise it was distributed relatively evenly throughout the brain in sparse amounts. Vimentin, on the other hand, was rarely detected in the brains of control animals, with noticeable staining located only in ependymal cells. For GFAP and Emx1 experimental brains, though, staining for both GFAP and vimentin was significantly increased compared to controls. The majority of this increased GFAP staining in mutant brains occurred in areas subject to *Ccm3* deletion. For the GFAP strain of animals these regions included the cerebellar and cerebral cortices as well as subcortical structures such as the basal ganglia and hippocampus. In the Emx1 strain, increased levels of staining were limited to the cerebral cortex and hippocampal formation (Figure 8). For vimentin, the majority of the increased staining in both the GFAP and Emx1 experimental animals was located in the cortex and hippocampal formation (Figure 9).

In addition to these widespread increases in astrocyte staining throughout affected brain areas of mutant animals, local staining increases in GFAP were also seen surrounding lesions. Areas of heavy staining were noted in the immediate vicinity of cavernomas, fully circumscribing the lesions and extending into the surrounding tissue (Figure 10).

Connexin43 Staining

Connexin43 is a protein found in gap junctions connecting the foot processes of astrocytes comprising the BBB. As such it plays an important role in cell signaling across this barrier [12]. In situ hybridization was used to detect the presence of connexin43 in both control and experimental animal brains, and resulting staining patterns of the different brains were compared (Figure 11). Overall staining for connexin43 was decreased in experimental animals when compared to controls in both GFAP as well as in Emx1 strains. Affected areas again appear to be limited to regions and structures in which *Ccm3* was deleted. Not only were these results seen globally throughout the brain as an overall decrease in staining density, but they were also seen locally in the area immediately surrounding lesions. These regions immediately adjacent to cavernomas were completely devoid of connexin43 staining.

Aquaporin 4 Staining

Aquaporin 4 is a water channel seen in astrocytic foot processes in direct contact with capillaries of the BBB. In situ hybridization was used to detect the presence of Aquaporin 4 RNA in control and experimental mice brains, and these results compared among the different animal types (Figure 12). In control brains, Aquaporin 4 staining was seen throughout most brain structures, especially in the hippocampal formation and midbrain. Regions in which staining was heaviest seemed to parallel areas of heaviest connexin43 staining, consisting with findings of another group that have looked at mRNA staining of both of these molecules [58]. In experimental animals, Aquaporin 4

staining took on a similar pattern in terms of the structures in which it was expressed, but the overall amount of staining appeared to be less. These results were true for both GFAP and Emx1 animal strains.

DISCUSSION

Ccm3 neural conditional knock-out mice survive embryogenesis and develop lesions resembling human CCMs, providing an animal model through which the pathophysiology of this devastating disease can be studied. In this particular study, the brains of these mice were examined and compared to those of control animals to determine differences that exist between the two. Although few animals in which *Ccm3* was deleted from GFAP-expressing cells and their progeny survived into adulthood, mice lacking *Ccm3* from Emx1-expressing cells and their progeny almost always survived, with the oldest mouse currently being over 16 months of age.

Aside from these differences in lifespan, which are likely attributable to the deletion of *Ccm3* from cerebellar cells of the GFAP animals given the behavioral phenotype seen in these mice, few differences were noted between the GFAP and Emx1 animal strains. Morphologically both strains were noted to have relatively large brains and small body sizes when compared to control animals, and both strains also developed lesions resembling human cavernomas in brain regions where *Ccm3* had been deleted. The Nissl and in situ hybridization staining patterns were also similar for both strains, with the only difference in staining between the two animal lines relating to the different brain regions targeted by these two different promoters. Unlike the Emx1 promoter, which is expressed specifically in cells of the neocortex and hippocampus, the GFAP promoter is also expressed in cells of the cerebellum and other subcortical structures, causing changes to be seen in these locations as well as those areas seen in Emx1 animals. It therefore

seems likely that Ccm3 is playing a similar role in both of these animals, and further characterizing this role is possible by comparing the differences between these experimental animals and normal controls.

The first major differences observed between control and experimental animals were morphological, relating to differences in the brain and body sizes seen in control and experimental animals. The weights of these animals' brains and bodies were used to quantify these differences. Although the sample size is small, the graphs of the brain weight data show a clear difference between control and experimental animals' brains beginning in the second week of postnatal development, with experimental brains weighing more than those of controls. This difference continues into adulthood, where, with larger sample sizes allowing for calculation of statistical significance, a significant difference is appreciated. At the same time, results show that the body weights of experimental animals are less than those of controls beginning very early in postnatal life, and again this trend persists into adulthood, where it is statistically significant. Considering these two trends together shows that the increased brain weight is an absolute increase rather than one that is relative to body size. In fact, given that the body weights of experimental animals is decreased compared to those of controls further shows that the increased brain weight is an absolute and not a relative increase because the weights of both of these variables are moving in opposite directions. The relative increase in brain size in these animals is therefore even greater, making this increase in weight even more substantial.

Although size changes in many regions are likely responsible for the overall weight increase in experimental brains, further comparison of control and experimental brains that have been sectioned in the coronal plane consistently reveal gross differences between particular structures. The most obvious of these regions is the cerebral cortex, which appears to be much thicker in experimental brains. Another area in which gross differences are noted between experimental and control brain sizes is in the ventricular system, where experimental animals are noted to have a much larger ventricles than those of controls, especially with respect to the lateral ventricles, which are extremely dilated in experimental animals. While these observations can easily be made thanks to the relatively large size of these structures even in control animals, other size differences are likely to be present that could not be noted on a gross level. Further comparisons between control and experimental brains made on a smaller scale would likely yield even more differences.

One of the main goals of this study was to provide further insight into what is accounting for these phenotypic changes in the brains of experimental mice. Since in vitro studies have shown that Ccm3 is both necessary and sufficient for induction of apoptosis [53], one hypothesis to explain these findings is that this size increase is secondary to an increased number of cells. Since apoptosis is not occurring as it normally would, more cells are surviving and therefore increasing the size and mass of the animals' brains.

Other techniques were also used to further test this hypothesis. Analysis of brain cytoarchitecture using Nissl staining was one such method. Staining patterns in the cerebral cortex were of particular interest since coronal sections through mutant brains demonstrate a dramatic size increase in this structure when compared to controls. When viewing the staining results, however, it was difficult to compare the cell number or staining intensity between the experimental and control brains because of the vastly different organization of these structures in the two groups. The cerebral cortex of control brains consisted of well-defined cortical layers, while experimental brains lacked this rigid layout. There were no defined cortical layers in mutant brains, and cells in this region of experimental brains also seemed to be arranged less densely than cells in the control cortex. Therefore, despite not being able to comment on differences in absolute cell numbers between the cortexes of control and experimental brains, these staining patterns still provide insight on differences between the brains of these different animals. More specifically, these observations suggest that the absence of *Ccm3* somehow causes the large, disordered cortex seen in experimental brains. One potential explanation for these cortical changes is a decrease in apoptosis in brains of experimental animals. Prior research has shown that apoptosis is an important determinant in both the size of the CNS during development as well as the appropriate size and shape of the forebrain in mammals [59, 60]. CCM3 has already been shown to have an apoptotic role in vitro. Overexpression of CCM3 in endothelial cells lines has been shown to induce apoptosis in vitro, and siRNA inhibition of CCM3 in endothelial cells results in lower levels of cell death [53]. Furthermore, astrocytes isolated from *GFAP*-Cre;$Ccm3^{lox/lox}$ animals are resistant to cycloheximide-induced apoptosis [61], and these mutant astrocytes also show

increased proliferation (A. Louvi, L. Chen, A. Two, H. Zhang, W. Min, and M. Günel: Loss of CCM3 function in neuroglia leads to cerebral cavernous malformations, *submitted*). Therefore, if CCM3 also has a role in inducing apoptosis in vivo, it could be responsible for the cortical changes seen in experimental mice.

To further investigate the hypothesis that CCM3 has a role in apoptosis in vivo, in situ hybridization was used to look for staining differences between control and experimental brains that might indicate increases in cellularity. The first in situ experiments done were for GFAP and vimentin, both markers of astrocytes. These results showed mRNA for both of these markers to be globally upregulated in mutant brain structures in which Ccm3 had been deleted when compared to control brains, suggesting an increase in astrocytes in these regions of experimental brains. Since vimentin is specifically upregulated in reactive astrocytes, these results also suggest the presence of reactive gliosis in experimental brains. In addition to providing a possible explanation for why mutant brains are larger than those of controls, the reactive gliosis also provides some insight into the molecular changes that may be occurring in these animals' brains. Reactive gliosis is the brain's normal physiologic response to any type of insult, including infection, degeneration, ischemia, and exposure to toxins. It occurs when, following one of these types of injury, astrocytes at the site of the insult hypertrophy and sometimes even proliferate to form a scar-like structure that limits the extent of the injury's spread. The reactive astrocytosis seen in experimental brains therefore suggests some form of injury in these animals' brains. Given that these animals develop vascular lesions, ischemia seems like a probable source of the insult. Further comparison of the

vasculature of control and experimental animals supports this possibility. First, brains of experimental animals have a decreased density of blood vessels. In addition, vessels in experimental brains appear to be disorganized and to have an increased diameter when compared to vessels in control brains (Louvi et al., *submitted*). These findings support ischemia's role as a potential mechanism for reactive gliosis since it seems unlikely that these disordered vessels could adequately support the neurons and increased astrocytes of the larger experimental brains. Ischemia is therefore another possible mechanism of the reactive gliosis that occurs in these brains.

These differences in the vasculature of experimental brains as well as the probable presence of ischemia in these animals again highlight the presence of vascular deficits seen in these *Ccm3* conditional knock-out animals. In this animal model, however, *Ccm3* is only knocked-out from neurons and astrocytes, indicating that there must be some connection between the cells targeted by the knock-out and those comprising the vasculature. Given that astrocytes and endothelial cells communicate with each other by signaling across the BBB, the neurovascular unit is implicated as a potential source of dysfunction in experimental animals.

To further investigate this concept that impairment at the level of the neurovascular unit is responsible for the changes in the brains of experimental animals, in situ hybridization was done to detect the mRNA of connexin43, a protein in gap junctions of the BBB, and aquaporin4, a water channel also found in the BBB. Compared to that seen in control

brains, the staining intensity of both connexin43 and aquaporin4 mRNA was greatly diminished in experimental brains, suggesting a decrease in these BBB gap junctions and water channels respectively. This result is even more significant when taking into account the previously discussed finding that experimental brains have an increase in activated astrocytes compared to controls. With more of these astrocytes, one would expect more of both connexin43-containing gap junctions and aquaporin 4 water channels to be necessary in experimental brains in order to fulfill their respective roles, which involve maintaining integrity and signaling between different components of the BBB. Without the correct number and distribution of these channels, the integrity of individual neurovascular units, including communication across them, may be compromised. Over time, these deficits could potentially lead to ischemia, which would then be accompanied by the reactive gliosis seen in experimental animals.

In situ hybridization results must be interpreted with caution, though. The findings presented are all qualitative rather than quantitative, and therefore care must be made when drawing conclusions from these results. To help minimize discrepancies between staining intensities for control and experimental brains, all tissue was handled in the same fashion. Both control and experimental brain sections for each given marker were developed for the same amount of time so that they were exposed equally to the probe. Furthermore, when viewing and imaging the stained sections, the light source was kept constant so as not to affect the brightness of the resulting images. Nonetheless, the current findings could be confirmed using Western blot to analyze the protein content of the proteins of interest in control and experimental brains.

Assuming that this hypothesis of disorganization at the level of the neurovascular unit is correct, several questions remain to be answered. The first of these questions is what causes CCMs to develop. One possible explanation for lesion formation relates to neural injury. This hypothesis is supported by the focal nature of lesions, as well as their age dependence. The youngest animals in which lesions were seen were three weeks old. In all of these young animals with lesions, hydrocephalus was also present. No lesions were found in animals this young without hydrocephalus, but lesions were routinely seen in animals without hydrocephalus that were over a few months old. These findings suggest the possibility that an underlying injury such as stress caused by hydrocephalus was seen in these animals, and given the existing mutation in these animals' brains, the addition of this insult caused the development of a CCM. This theory can be tested by selectively injuring the brains of mutant animals at a young age such as by sacrificing one of the main arteries to the brain and later examining these brains for the presence of cavernomas. If this injury theory is true, these animals will develop cavernomas within a short period of time following the vascular insult, and multiple lesions may even be seen depending on the severity of the ischemia.

This theory of a focal insult being necessary for lesion development also helps answer another question regarding experimental animals, which is why more lesions are not seen per animal. Since the reactive astrocytosis and changes in the neurovascular unit in experimental animals are widespread and seen throughout areas of the brain affected by

the Ccm3 deletion, it is unclear why more lesions are not seen per animal. Although a few animals had multiple lesions, the majority only had one lesion. With such global changes in the brain, one would expect many more lesions to develop in experimental brains. If both a focal insult and the widespread vascular changes seen in experimental animals are necessary for lesion development, CCM formation would not only be less common among experimental animals, but it would also be more likely to occur as animals aged, which is exactly what was observed among animals studied.

Like any animal model, though, these Ccm3 conditional knock-out mice are not without their limitations. Widespread changes such as the reactive gliosis seen throughout experimental brains are not recognized as being a part of the disease phenotype in humans. This difference could potentially be accounted for by differences in Ccm3 expression between humans and mice, but current studies of CCM3 expression suggest it is similar in mice and humans [52]. Another possible explanation for the different phenotypes seen in the human disease and the experimental model is related to the two-hit hypothesis of the disease pathogenesis in humans. According to this model, humans with the inherited form of the disease have a germline mutation in one of their two *CCM3* alleles, leaving one functioning copy of the allele. Focal lesions develop when a second sporadic hit, or mutation, affects the remaining intact *CCM3* allele, completely inactivating *CCM3* in these specific cells only. In the mouse model, however, both copies of the *Ccm3* allele are knocked-out, completely inactivating this gene in all cells targeted by the promoter. These targeted cells in these animals therefore lack the one functioning copy of *CCM3* seen in most cells of human patients, perhaps explaining the

more widespread neural pathophysiology seen in the experimental model. Nonetheless, given that these animals develop lesions that resemble human cavernomas after knocking-out one of the genes implicated in cavernoma development in humans, this animal model still seems appropriate for studying lesion development and the role of Ccm3 in the pathophysiology of this disease, potentially allowing for results from this model to be generalized to humans, and thus potentially implicating dysfunction at the neurovascular unit as also contributing to disease pathophysiology in humans.

REFERENCES

1. Clatterbuck, R.E., et al., *Ultrastructural and immunocytochemical evidence that an incompetent blood-brain barrier is related to the pathophysiology of cavernous malformations.* J Neurol Neurosurg Psychiatry, 2001. **71**(2): p. 188-92.
2. Otten, P., et al., *[131 cases of cavernous angioma (cavernomas) of the CNS, discovered by retrospective analysis of 24,535 autopsies]*. Neurochirurgie, 1989. **35**(2): p. 82-3, 128-31.
3. Robinson, J.R., I.A. Awad, and J.R. Little, *Natural history of the cavernous angioma.* J Neurosurg, 1991. **75**(5): p. 709-14.
4. Sage, M.R., et al., *Cavernous haemangiomas (angiomas) of the brain: clinically significant lesions.* Australas Radiol, 1993. **37**(2): p. 147-55.
5. Giombini, S. and G. Morello, *Cavernous angiomas of the brain. Account of fourteen personal cases and review of the literature.* Acta Neurochir (Wien), 1978. **40**(1-2): p. 61-82.
6. Lonjon, M., et al., *[Intracranial cavernoma. 30 cases]*. Presse Med, 1993. **22**(21): p. 990-4.
7. Aiba, T., et al., *Natural history of intracranial cavernous malformations.* J Neurosurg, 1995. **83**(1): p. 56-9.
8. Del Curling, O., Jr., et al., *An analysis of the natural history of cavernous angiomas.* J Neurosurg, 1991. **75**(5): p. 702-8.

9. Raychaudhuri, R., H.H. Batjer, and I.A. Awad, *Intracranial cavernous angioma: a practical review of clinical and biological aspects.* Surg Neurol, 2005. **63**(4): p. 319-28; discussion 328.

10. Clatterbuck, R.E., et al., *Dynamic nature of cavernous malformations: a prospective magnetic resonance imaging study with volumetric analysis.* J Neurosurg, 2000. **93**(6): p. 981-6.

11. Maraire, J.N. and I.A. Awad, *Intracranial cavernous malformations: lesion behavior and management strategies.* Neurosurgery, 1995. **37**(4): p. 591-605.

12. Simard, J.M., et al., *Cavernous angioma: a review of 126 collected and 12 new clinical cases.* Neurosurgery, 1986. **18**(2): p. 162-72.

13. Samii, M., et al., *Surgical management of brainstem cavernomas.* J Neurosurg, 2001. **95**(5): p. 825-32.

14. Brown, R.D., Jr., et al., *Natural history, evaluation, and management of intracranial vascular malformations.* Mayo Clin Proc, 2005. **80**(2): p. 269-81.

15. Hasegawa, T., et al., *Long-term results after stereotactic radiosurgery for patients with cavernous malformations.* Neurosurgery, 2002. **50**(6): p. 1190-7; discussion 1197-8.

16. Kondziolka, D., et al., *Reduction of hemorrhage risk after stereotactic radiosurgery for cavernous malformations.* J Neurosurg, 1995. **83**(5): p. 825-31.

17. Amin-Hanjani, S., et al., *Stereotactic radiosurgery for cavernous malformations: Kjellberg's experience with proton beam therapy in 98 cases at the Harvard Cyclotron.* Neurosurgery, 1998. **42**(6): p. 1229-36; discussion 1236-8.

18. Karlsson, B., et al., *Radiosurgery for cavernous malformations.* J Neurosurg, 1998. **88**(2): p. 293-7.

19. Pollock, B.E., et al., *Stereotactic radiosurgery for cavernous malformations.* J Neurosurg, 2000. **93**(6): p. 987-91.

20. Gewirtz, R.J., et al., *Pathological changes in surgically resected angiographically occult vascular malformations after radiation.* Neurosurgery, 1998. **42**(4): p. 738-42; discussion 742-3.

21. Hayman, L.A., et al., *Familial cavernous angiomas: natural history and genetic study over a 5-year period.* Am J Med Genet, 1982. **11**(2): p. 147-60.

22. Cave-Riant, F., et al., *Spectrum and expression analysis of KRIT1 mutations in 121 consecutive and unrelated patients with Cerebral Cavernous Malformations.* Eur J Hum Genet, 2002. **10**(11): p. 733-40.

23. Rigamonti, D., et al., *Cerebral cavernous malformations. Incidence and familial occurrence.* N Engl J Med, 1988. **319**(6): p. 343-7.

24. Dubovsky, J., et al., *A gene responsible for cavernous malformations of the brain maps to chromosome 7q.* Hum Mol Genet, 1995. **4**(3): p. 453-8.

25. Gil-Nagel, A., et al., *Familial cerebral cavernous angioma: a gene localized to a 15-cM interval on chromosome 7q.* Ann Neurol, 1996. **39**(6): p. 807-10.

26. Gunel, M., et al., *Mapping a gene causing cerebral cavernous malformation to 7q11.2-q21.* Proc Natl Acad Sci U S A, 1995. **92**(14): p. 6620-4.

27. Johnson, E.W., et al., *Refined localization of the cerebral cavernous malformation gene (CCM1) to a 4-cM interval of chromosome 7q contained in a well-defined YAC contig.* Genome Res, 1995. **5**(4): p. 368-80.

28. Notelet, L., et al., *Familial cavernous malformations in a large French kindred: mapping of the gene to the CCM1 locus on chromosome 7q.* J Neurol Neurosurg Psychiatry, 1997. **63**(1): p. 40-5.

29. Labauge, P., et al., *Hereditary cerebral cavernous angiomas: clinical and genetic features in 57 French families. Societe Francaise de Neurochirurgie.* Lancet, 1998. **352**(9144): p. 1892-7.

30. Verlaan, D.J., A.M. Siegel, and G.A. Rouleau, *Krit1 missense mutations lead to splicing errors in cerebral cavernous malformation.* Am J Hum Genet, 2002. **70**(6): p. 1564-7.

31. Chen, D.H., et al., *Cerebral cavernous malformation: novel mutation in a Chinese family and evidence for heterogeneity.* J Neurol Sci, 2002. **196**(1-2): p. 91-6.

32. Couteulx, S.L., et al., *A novel KRIT1/CCM1 truncating mutation in a patient with cerebral and retinal cavernous angiomas.* Arch Ophthalmol, 2002. **120**(2): p. 217-8.

33. Davenport, W.J., et al., *CCM1 gene mutations in families segregating cerebral cavernous malformations.* Neurology, 2001. **56**(4): p. 540-3.

34. Zhang, J., et al., *Mutations in KRIT1 in familial cerebral cavernous malformations.* Neurosurgery, 2000. **46**(5): p. 1272-7; discussion 1277-9.

35. Laurans, M.S., et al., *Mutational analysis of 206 families with cavernous malformations.* J Neurosurg, 2003. **99**(1): p. 38-43.

36. Gault, J., et al., *Biallelic somatic and germ line CCM1 truncating mutations in a cerebral cavernous malformation lesion.* Stroke, 2005. **36**(4): p. 872-4.

37. Chishti, A.H., et al., *The FERM domain: a unique module involved in the linkage of cytoplasmic proteins to the membrane.* Trends Biochem Sci, 1998. **23**(8): p. 281-2.

38. Zawistowski, J.S., et al., *KRIT1 association with the integrin-binding protein ICAP-1: a new direction in the elucidation of cerebral cavernous malformations (CCM1) pathogenesis.* Hum Mol Genet, 2002. **11**(4): p. 389-96.

39. Zhang, J., et al., *Interaction between krit1 and icap1alpha infers perturbation of integrin beta1-mediated angiogenesis in the pathogenesis of cerebral cavernous malformation.* Hum Mol Genet, 2001. **10**(25): p. 2953-60.

40. Zawistowski, J.S., et al., *CCM1 and CCM2 protein interactions in cell signaling: implications for cerebral cavernous malformations pathogenesis.* Hum Mol Genet, 2005. **14**(17): p. 2521-31.

41. Chang, D.D., et al., *ICAP-1, a novel beta1 integrin cytoplasmic domain-associated protein, binds to a conserved and functionally important NPXY sequence motif of beta1 integrin.* J Cell Biol, 1997. **138**(5): p. 1149-57.

42. Zhang, X.A. and M.E. Hemler, *Interaction of the integrin beta1 cytoplasmic domain with ICAP-1 protein.* J Biol Chem, 1999. **274**(1): p. 11-9.

43. Bloch, W., et al., *Beta 1 integrin is essential for teratoma growth and angiogenesis.* J Cell Biol, 1997. **139**(1): p. 265-78.

44. Brooks, P.C., *Role of integrins in angiogenesis.* Eur J Cancer, 1996. **32A**(14): p. 2423-9.

45. Hilder, T.L., et al., *Proteomic identification of the cerebral cavernous malformation signaling complex.* J Proteome Res, 2007. **6**(11): p. 4343-55.

46. Voss, K., et al., *CCM3 interacts with CCM2 indicating common pathogenesis for cerebral cavernous malformations.* Neurogenetics, 2007. **8**(4): p. 249-56.

47. Uhlik, M.T., et al., *Rac-MEKK3-MKK3 scaffolding for p38 MAPK activation during hyperosmotic shock.* Nat Cell Biol, 2003. **5**(12): p. 1104-10.

48. Guzeloglu-Kayisli, O., et al., *KRIT1/cerebral cavernous malformation 1 protein localizes to vascular endothelium, astrocytes, and pyramidal cells of the adult human cerebral cortex.* Neurosurgery, 2004. **54**(4): p. 943-9; discussion 949.

49. Whitehead, K.J., et al., *Ccm1 is required for arterial morphogenesis: implications for the etiology of human cavernous malformations.* Development, 2004. **131**(6): p. 1437-48.

50. Plummer, N.W., et al., *Loss of p53 sensitizes mice with a mutation in Ccm1 (KRIT1) to development of cerebral vascular malformations.* Am J Pathol, 2004. **165**(5): p. 1509-18.

51. Plummer, N.W., et al., *Neuronal expression of the Ccm2 gene in a new mouse model of cerebral cavernous malformations.* Mamm Genome, 2006. **17**(2): p. 119-28.

52. Tanriover, G., et al., *PDCD10, the gene mutated in cerebral cavernous malformation 3, is expressed in the neurovascular unit.* Neurosurgery, 2008. **62**(4): p. 930-8; discussion 938.

53. Chen, L., et al., *Apoptotic functions of PDCD10/CCM3, the gene mutated in cerebral cavernous malformation 3.* Stroke, 2009. **40**(4): p. 1474-81.

54. Schlaeger, T.M., et al., *Uniform vascular-endothelial-cell-specific gene expression in both embryonic and adult transgenic mice.* Proc Natl Acad Sci U S A, 1997. **94**(7): p. 3058-63.

55. Malatesta, P., et al., *Neuronal or glial progeny: regional differences in radial glia fate.* Neuron, 2003. **37**(5): p. 751-64.

56. Zhuo, L., et al., *hGFAP-cre transgenic mice for manipulation of glial and neuronal function in vivo.* Genesis, 2001. **31**(2): p. 85-94.

57. Gorski, J.A., et al., *Cortical excitatory neurons and glia, but not GABAergic neurons, are produced in the Emx1-expressing lineage.* J Neurosci, 2002. **22**(15): p. 6309-14.

58. Micevych, P.E. and L. Abelson, *Distribution of mRNAs coding for liver and heart gap junction proteins in the rat central nervous system.* J Comp Neurol, 1991. **305**(1): p. 96-118.

59. Williams, R.W., R.C. Strom, and D. Goldowitz, *Natural variation in neuron number in mice is linked to a major quantitative trait locus on Chr 11.* J Neurosci, 1998. **18**(1): p. 138-46.

60. Haydar, T.F., et al., *The role of cell death in regulating the size and shape of the mammalian forebrain.* Cereb Cortex, 1999. **9**(6): p. 621-6.

61. Tsuchida, T., et al., *Cycloheximide induces apoptosis of astrocytes.* Pathol Int, 2002. **52**(3): p. 181-5.

FIGURES

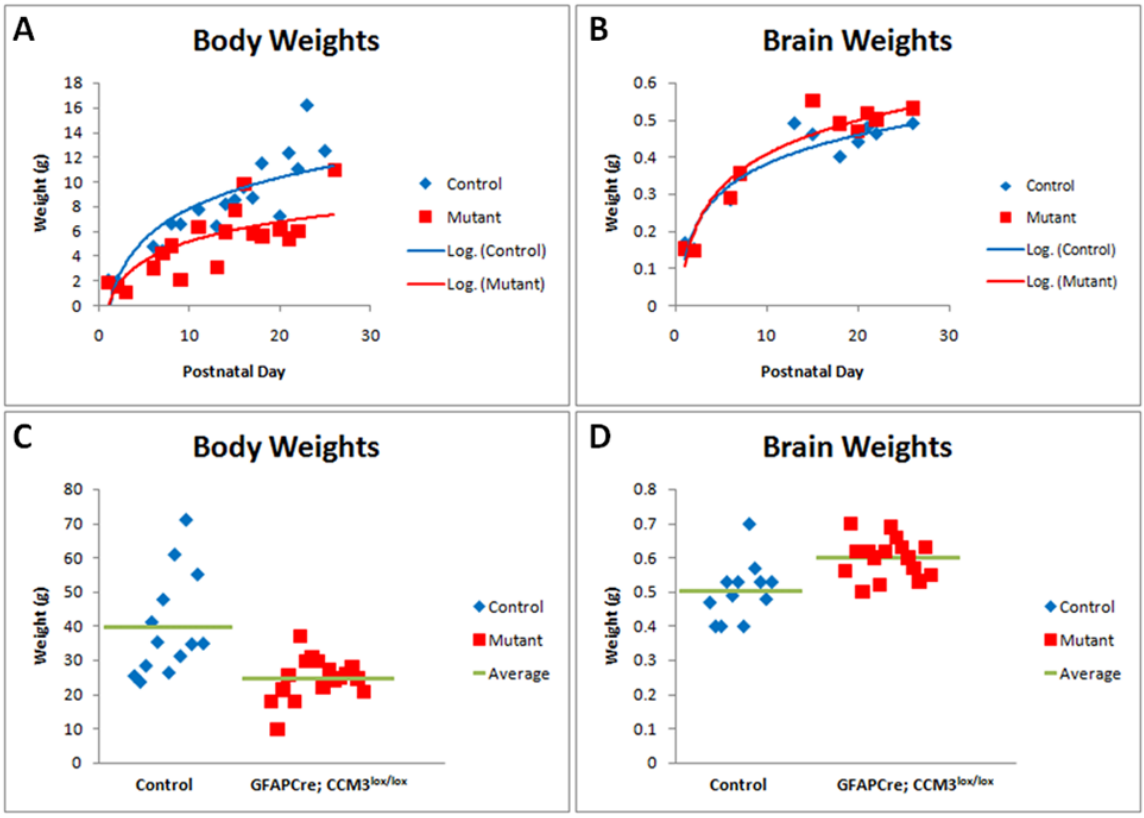

Figure 1: Graphs of average body (A) and brain (B) weights of control and experimental animals at various postnatal days, as well as body (C) and brain (D) weights of adult animals. Brain weights of experimental animals are noticeably greater than those of controls starting around the second week of postnatal life, a trend that continues into adulthood. Body weights of experimental animals are observed to be smaller than those of controls beginning early in development and this trend also continues into adulthood.

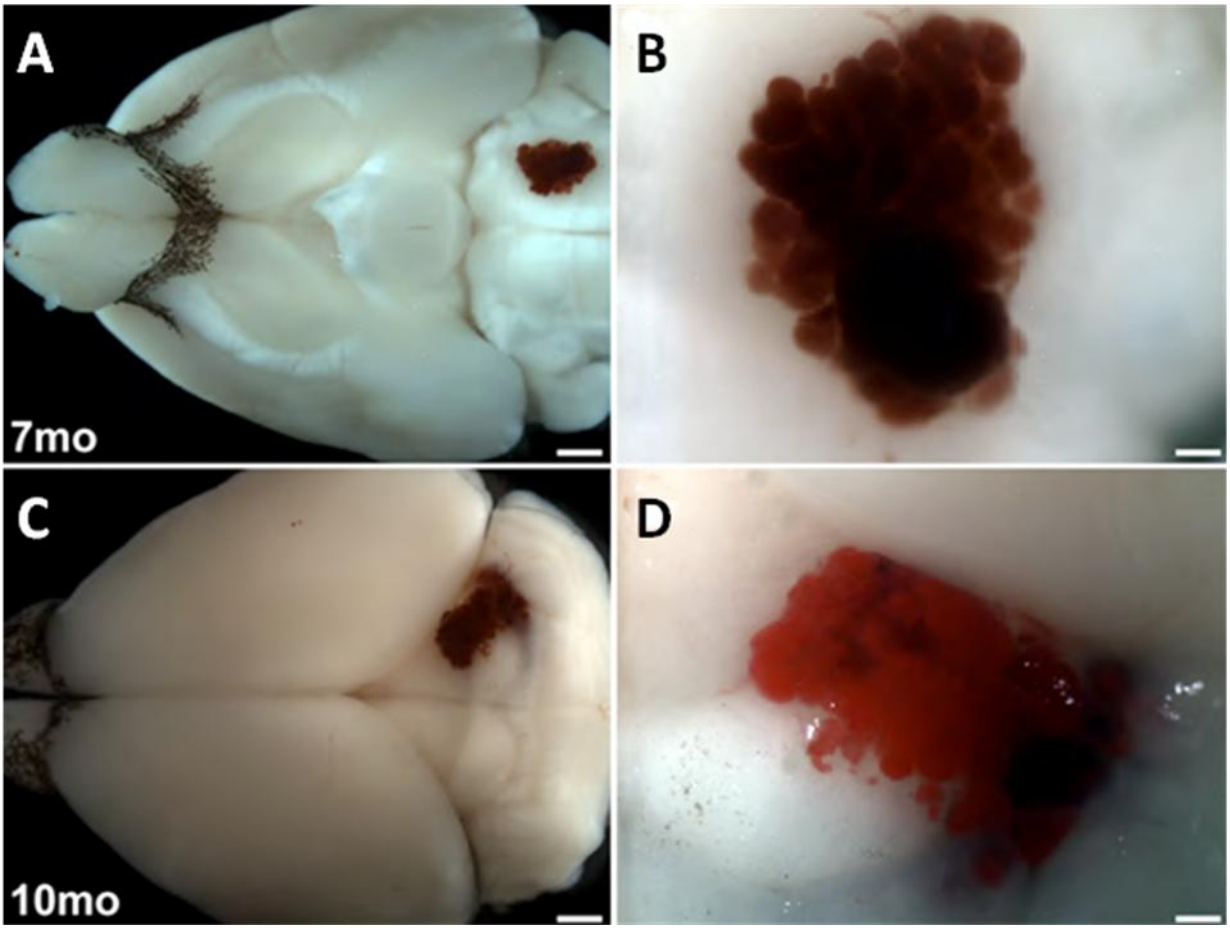

Figure 2: Images of lesions seen in the medulla (A and B) and in the dorsal midbrain (C and D) of GFAP mice. (B) and (D) are magnified images of the lesions seen in (A) and (C) respectively. Scale bars in (A) and (C) represent 1 mm, and those in (B) and (D) are 200 µm.

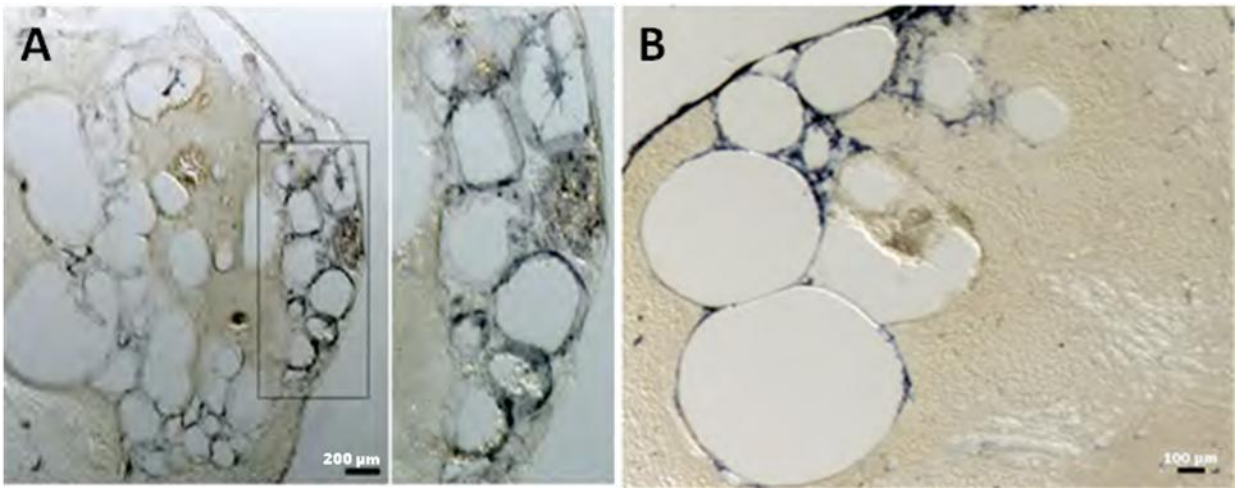

Figure 3: Lesion analysis using PECAM (A) and Igf2 (B) staining. PECAM staining of the lesion shows channels in the lesion lined by a single layer of endothelial cells. A higher magnification of the boxed region is shown just to the right of the main image. Igf2 staining shows mesenchymal cells surrounding but not within the lesion.

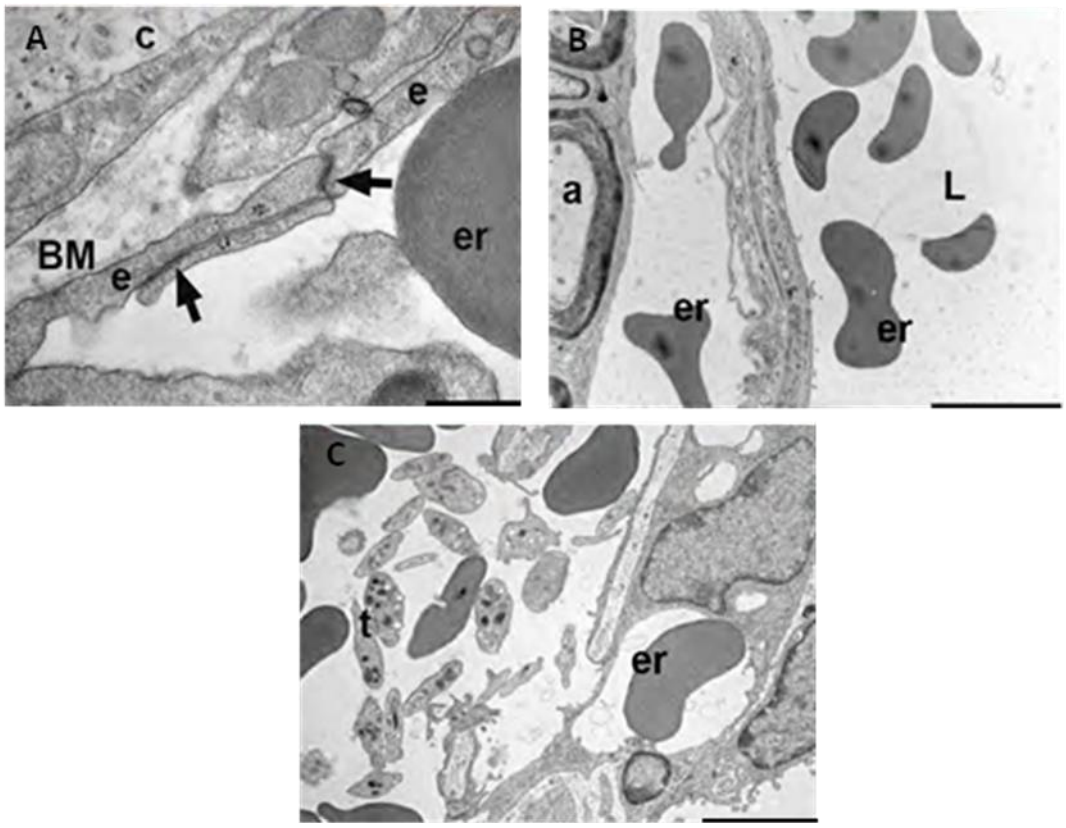

Figure 4: Lesion analysis using electron microscopy. In image (A), electron microscopy confirms the single layer of endothelial cells (e) comprising lesions, with tight junctions (arrows) joining these cells. An irregular basement membrane (BM) supported by connective tissue (c) is seen in the area surrounding lesions. In (B) and (C), erythrocytes (er) and platelets (t) are seen in the lumen of lesions (L), and erythrocytes are additionally seen abluminally. An axon (a) is also seen adjacent to the lesion in (B). Scale bars represent 500 nm in (A), 5 μm in (B), and 1 μm in (C).

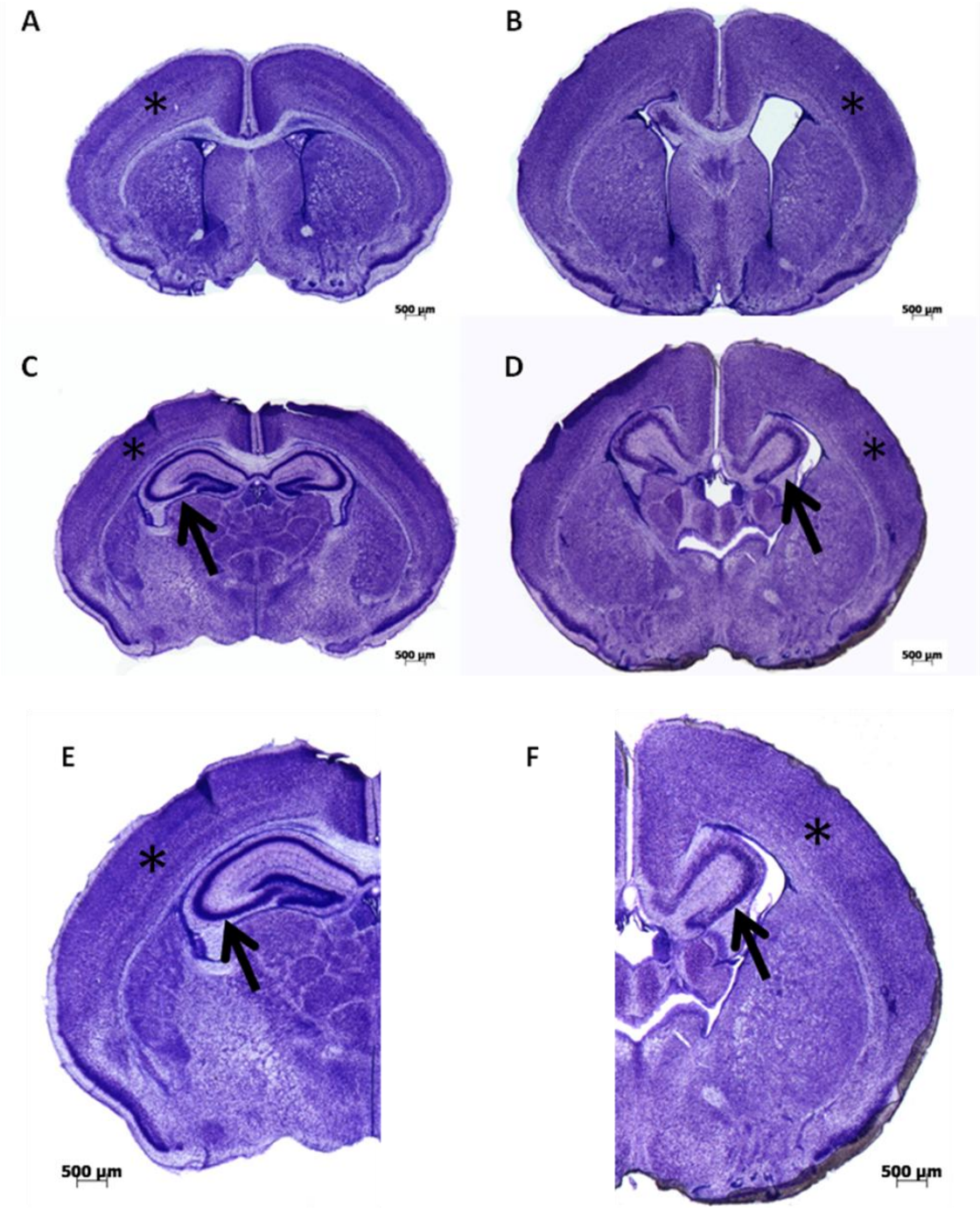

Figure 5: Nissl staining of representative control (A, C, E, and G) and GFAP experimental (B, D, F, H) brain sections. (A) and (C) are from a postnatal day seven control animal, while (B) and (D) correspond to approximately the same brain regions seen in (A) and (C) respectively, but in a postnatal day 13 experimental animal. (E) and

(F) are magnifications of (C) and (D) respectively. Asterisks mark the cortex, which is divided into discrete layers in control brains that are not seen in experimental brains. Arrows point to the hippocampal formation for each animal. Cells of the hippocampal formation are tightly packed into a discrete layer in control brains, while those of the experimental brains are loosely arranged and disorganized.

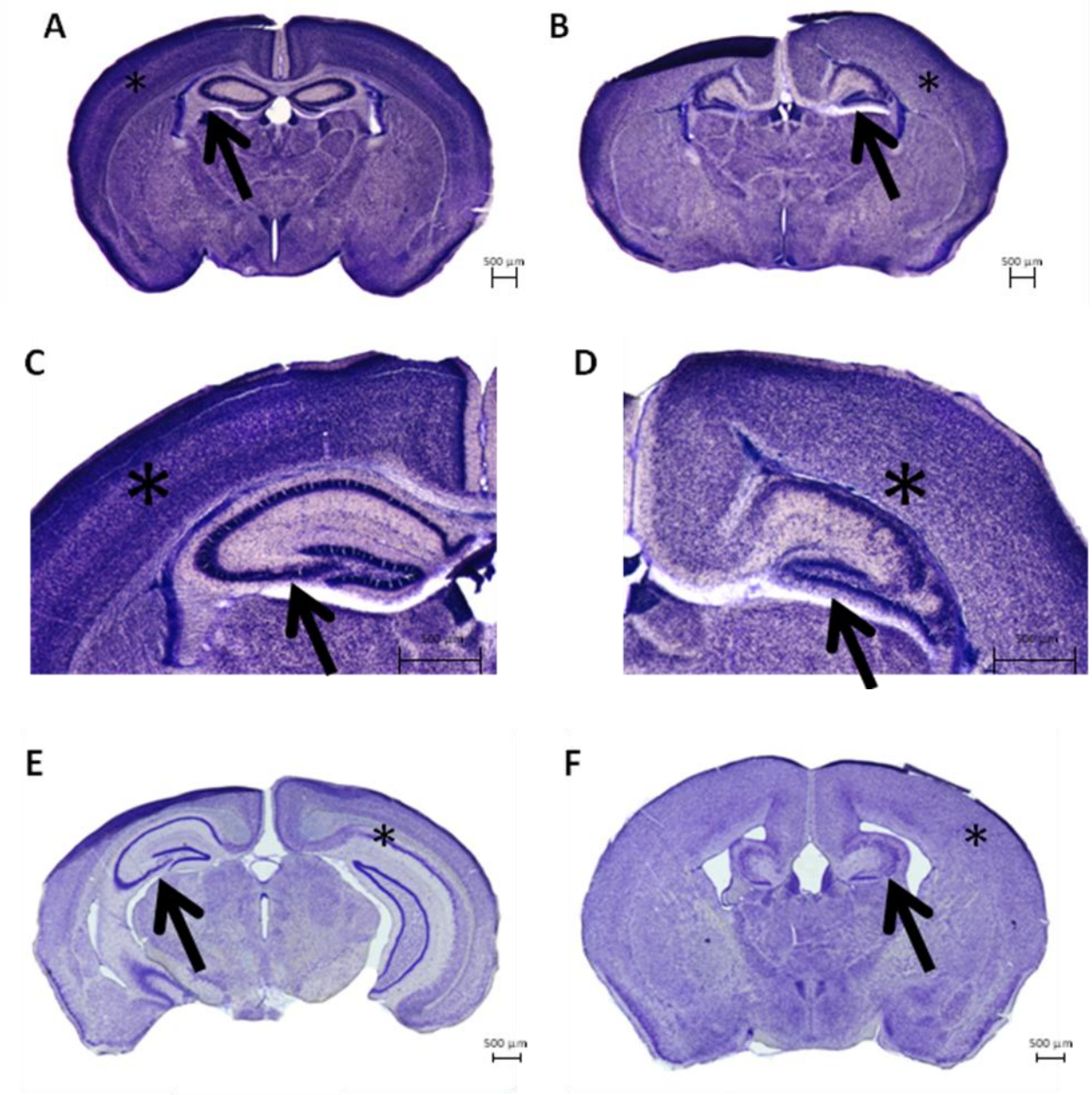

Figure 6: Nissl staining of representative control (A, C and E) and Emx1 experimental (B, D, and F) brain sections. (A) and (B) are taken at approximately equivalent levels of the brain of postnatal day 15 animals, while (C) and (D) respectively are magnifications of these sections to further highlight the cortical and hippocampal differences between the two. (E) and (F) are both from five month old animals. Asterisks mark the cortex, which is divided into discrete layers in control brains that are not seen in experimental

brains. Arrows point to the hippocampal formation for each animal. Cells of the hippocampal formation are tightly packed into a discrete layer in control brains, while those of the experimental brains are loosely arranged and disorganized.

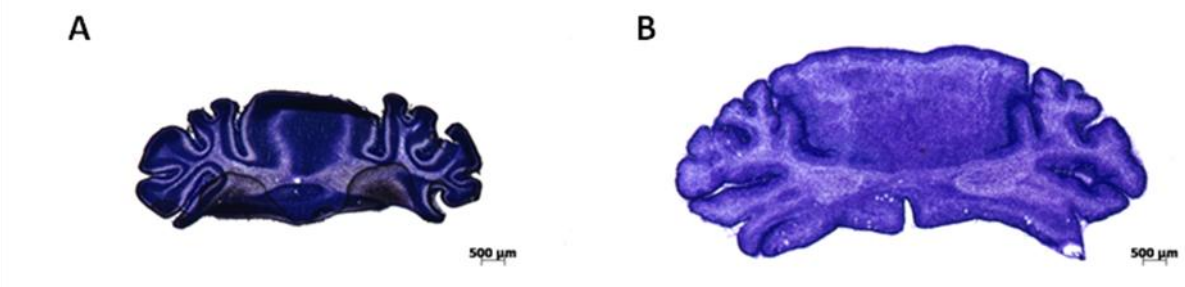

Figure 7: Nissl staining of the cerebellum of a representative postnatal day nine control (A) and postnatal day seven GFAP experimental (B) brain. Cells in the control brain appear to be arranged more closely and seem to form more well-defined layers.

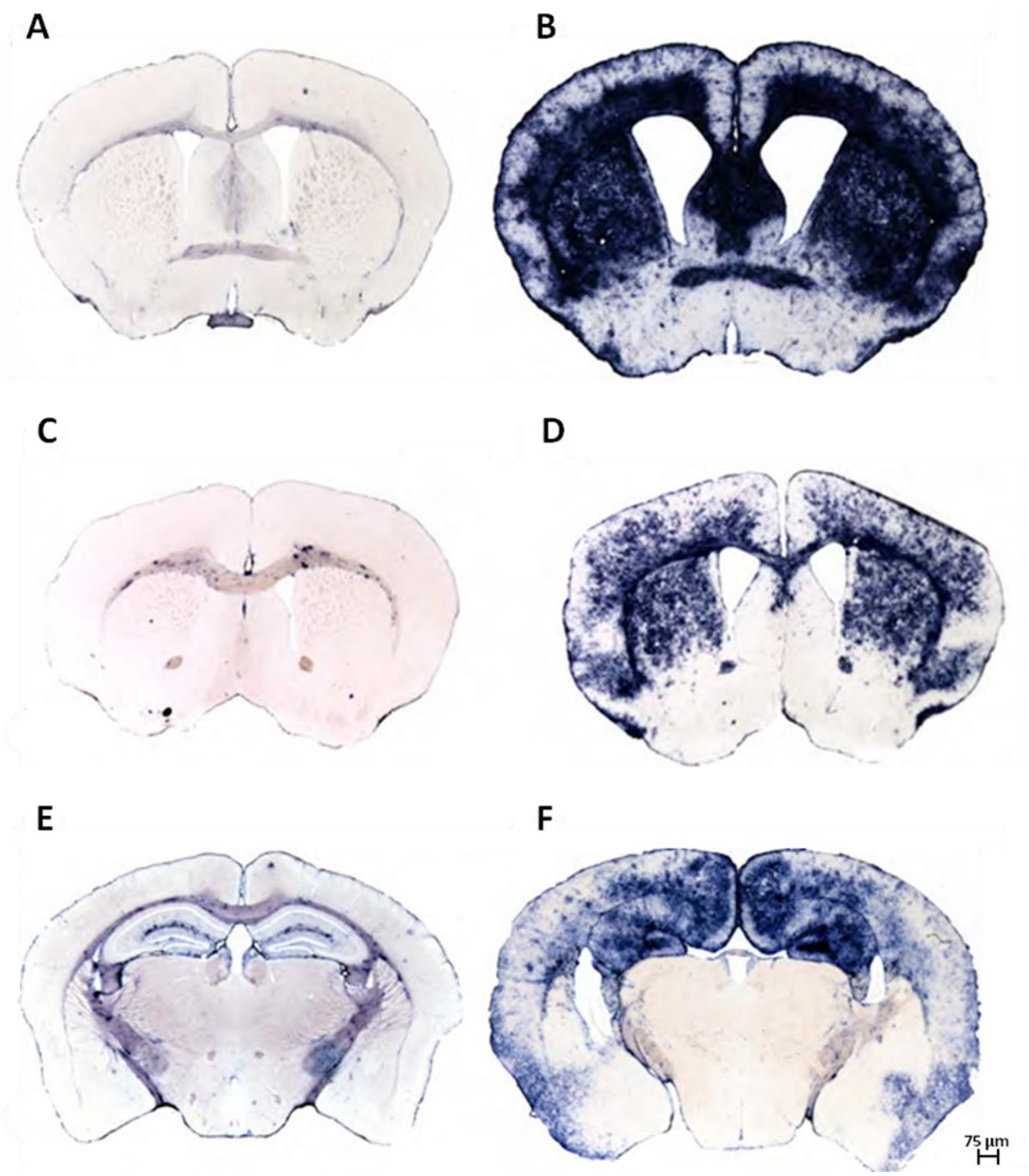

Figure 8: GFAP staining in control (A, C, and E) and GFAP (B and D) and Emx1 (F) experimental brains. (A) and (B) are from seven month old animals, and (C-F) from 10 month old animals. Staining in experimental brains is much more intense than that seen in control brains.

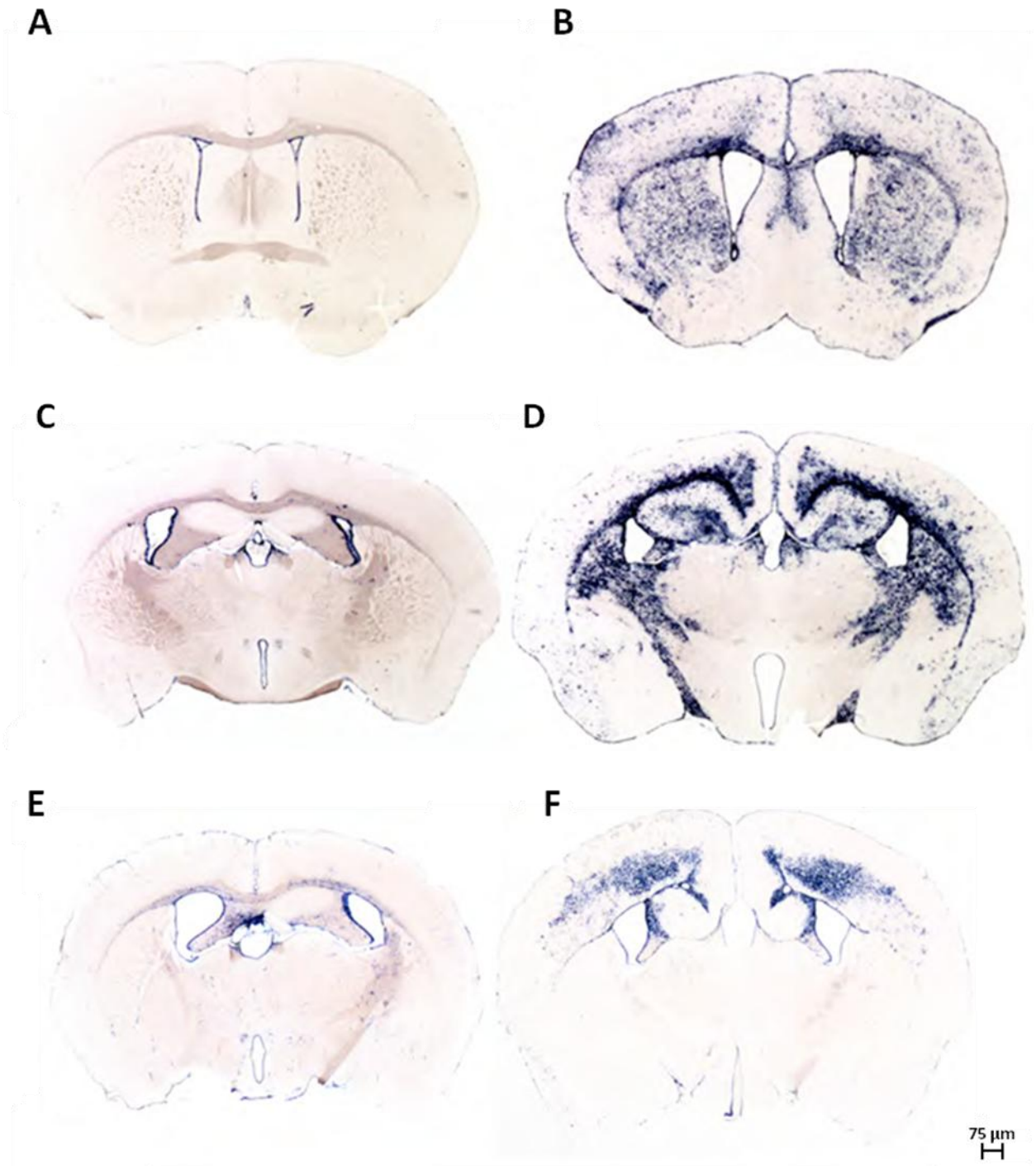

Figure 9: Vimentin staining in control (A, C, and E) and GFAP (B and D) and Emx1 (F) experimental brains. (A) and (B) are from nine month old animals, (C) and (D) from 10 month old animals, and (E) and (F) from five month old animals. Staining in experimental brains is much more intense than that seen in control brains.

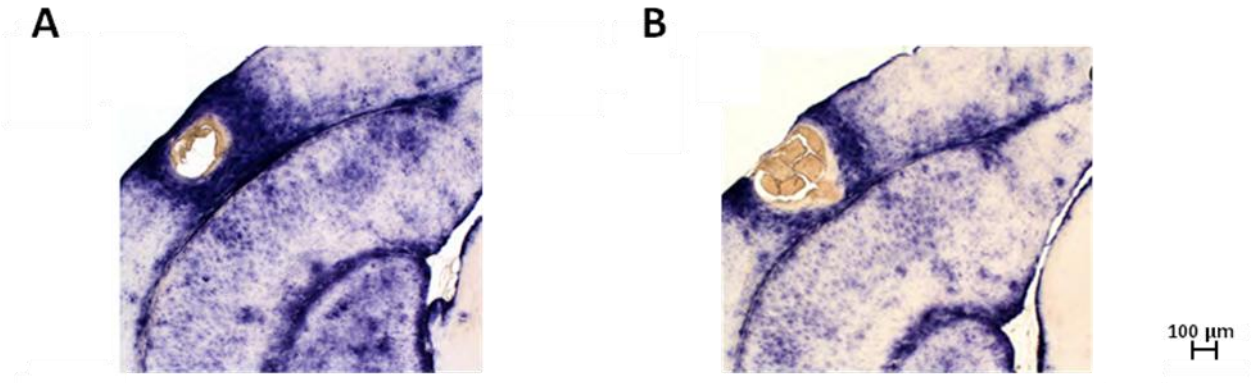

Figure 10: GFAP staining in two different five month old GFAP experimental brains containing lesions. Staining is darkest in regions immediately surrounding lesions.

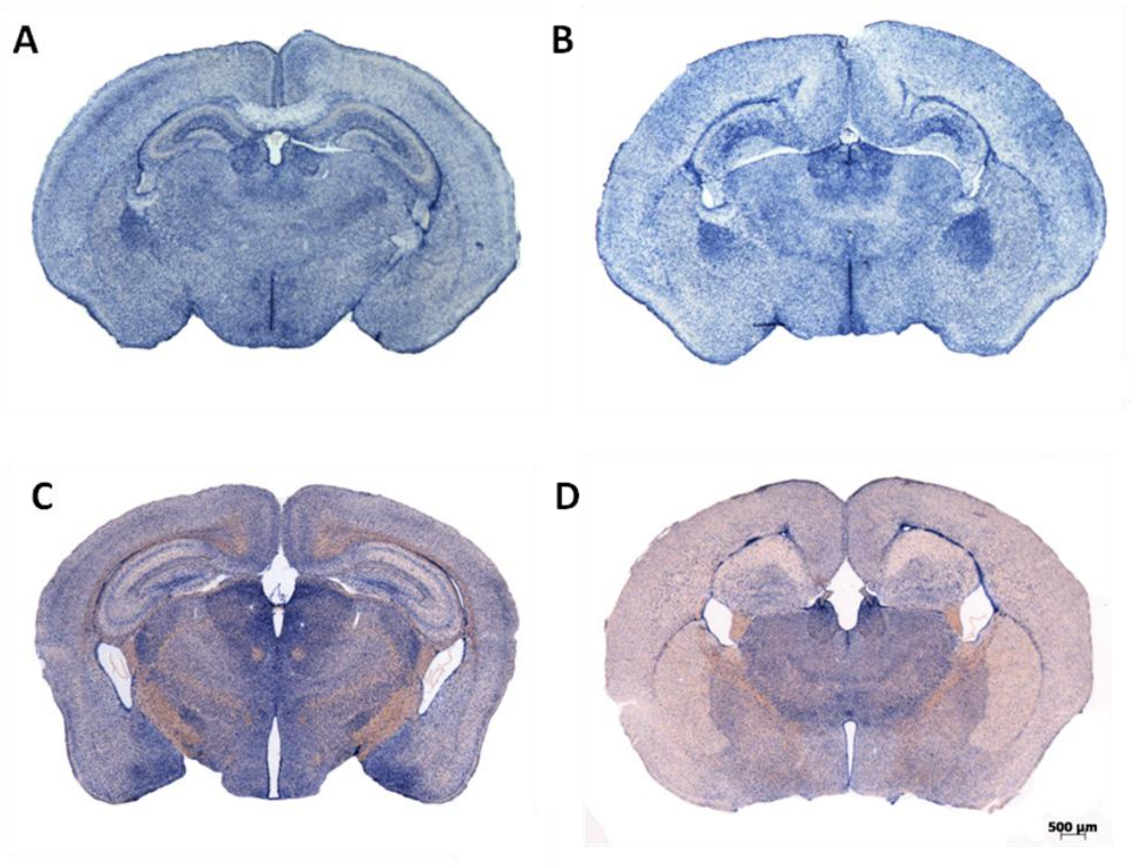

Figure 11: Connexin43 staining in postnatal day seven control (A) and Emx1 experimental (B) brains, as well as in five month old control (C) and Emx1 experimental (D) brains. Staining (blue) in control brains is darker than that of experimental brains.

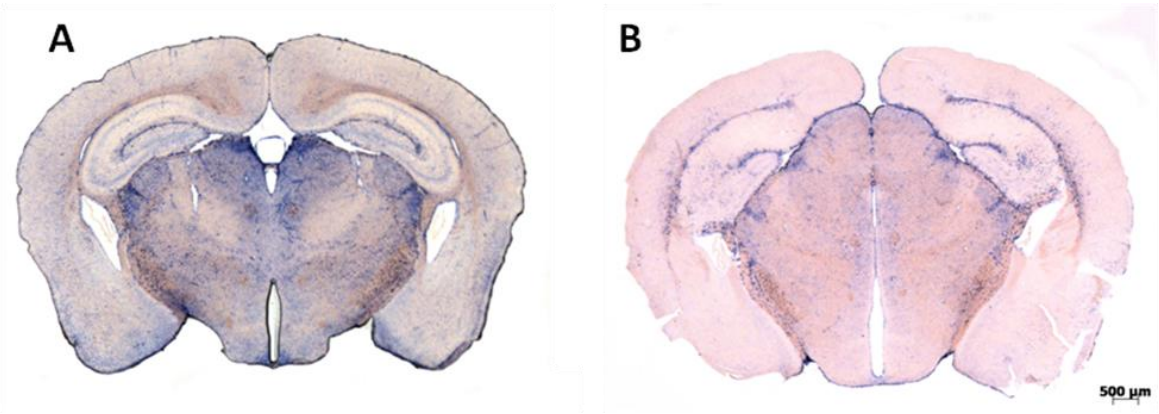

Figure 12: Aquaporin 4 staining in five month old control (A) and Emx1 experimental (B) brains. Staining (blue) in control brain is much more intense than that seen in the experimental brain.

TABLES

Postnatal Day	Control Animals		Experimental Animals	
	Average Weight (g)	Number of Animals	Average Weight (g)	Number of Animals
1	0.17	5	0.16	2
2	0.15	8	0.15	3
6	0.29	5	0.29	3
7	--	--	0.36	2
13	0.49	1	--	--
15	0.46	1	0.55	1
18	0.40	1	0.49	1
20	0.44	3	0.47	2
21	0.48	13	0.52	5
22	0.46	4	0.50	4
26	0.49	1	0.53	1

Table 1: Brain weights of non-adult control and GFAP experimental animals examined in this study, arranged by postnatal day.

Postnatal Day	Control Animals		Experimental Animals	
	Average Weight (g)	Number of Animals	Average Weight (g)	Number of Animals
1	2.02	17	1.88	4
2	1.94	8	1.57	3
3	--	--	1.13	2
6	4.74	8	3.06	4
7	4.40	15	4.23	6
8	6.60	4	4.86	10
9	6.56	8	2.1	1
11	7.75	6	6.4	2
13	6.40	2	3.16	2
14	8.18	5	5.98	4
15	8.52	6	7.70	4
16	9.55	2	9.88	2
17	8.70	3	5.87	3
18	11.49	1	5.64	2
20	7.20	3	6.15	2
21	12.33	14	5.43	6
22	11.03	7	6.00	6
25	12.50	1	--	--
26	--	--	10.95	2

Table 2: Body weights of non-adult control and GFAP experimental animals examined in this study, arranged by postnatal day.